GEOPHYSICS, VOL. 80, NO. 4 (JULY-AUGUST 2015); P. T175–T181, 7 FIGS.
10.1190/GEO2015-0001.1

A discontinuous collocated-grid implementation for high-order finite-difference modeling

Na Fan[1], Lian-Feng Zhao[2], Ying-Jie Gao[1], and Zhen-Xing Yao[2]

ABSTRACT

The discontinuous-grid method can greatly reduce the storage requirements and computational costs of finite-difference (FD) modeling for large-velocity-contrast models. However, traditional discontinuous-grid methods have to use interpolation when refining the wavefield in transition zones and would cause apparent artifacts. We have developed a new discontinuous collocated-grid scheme for high-order FD modeling. We refined the wavefield on a rotated coordinate system, where the interpolation is not required again. The horizontal and vertical spatial derivatives can be accurately converted into diagonal derivatives within the rotated coordinate system; thus, our scheme would be free of artifacts caused by improper interpolation. The ratio from coarse- to fine-grid spacing is restricted to 2^n for our scheme, where n is a positive integer. Numerical experiments demonstrate that the proposed discontinuous collocated-grid scheme reduces the artificial reflections by about two orders of magnitude compared to the interpolation scheme and yields a wavefield that is almost identical to that of the uniform-grid simulation. The rotated FD operator with arbitrary even-order accuracy is applied in the transition zones; thus, it significantly improves the spatial accuracy while saving computational cost.

INTRODUCTION

Large velocity contrasts extensively exist within the earth. In uniform-grid finite-difference (FD) modeling, the grid spacing is small enough to achieve sufficient accuracy, because the grid spacing is constrained by the lowest velocity in the model. This requirement would cause oversampling in high-velocity areas. To lower the storage requirements and reduce computational costs, a nonuniform-grid modeling technique has been widely applied using fine and coarse grids to discretize low- and high-velocity areas, respectively (e.g., Jastram and Tessmer, 1994; Moczo et al., 1996; Wang and Takenaka, 2001; Kang and Baag, 2004a; Wu et al., 2005; Zhang et al., 2008).

There are two primary types of nonuniform grid schemes, as shown in Figure 1. The shaded areas illustrate low-velocity regions with local fine gridding using continuous-grid (Figure 1a) and discontinuous-grid (Figure 1b) schemes. These two schemes are categorized according to whether they use interpolation to refine the wavefield in transition regions in which the fine and coarse grids overlap. The conventional FD operator depends on a few grid points in the horizontal and vertical directions that are usually located symmetrically around a central point at which the local derivative is computed. As shown in Figure 1a, there is no discontinuous point located on the grid line; consequently, a high-order FD operator can be applied over the entire region (e.g., Falk et al., 1996; Opršal and Zahradnik, 1999; Pitarka, 1999; Wu et al., 2005). As shown in Figure 1b, the low-velocity area is discretized using a fine grid and the interpolation is required to refine the wavefield from the coarse grid to the fine grid (e.g., Jastram and Behle, 1992; Jastram and Tessmer, 1994; Wang and Schuster, 1996; Liu et al., 2014). The continuous-grid scheme has accuracy similar to the traditional uniform-grid FD method using the fine grid, but it saves less computational cost compared with the discontinuous-grid scheme. Therefore, discontinuous-grid schemes are widely used because of their great flexibility and high efficiency (e.g., Aoi and Fujiwara, 1999; Hayashi et al., 2001; Wang et al., 2001; Kristek et al., 2010; Zhang et al., 2013).

However, traditional discontinuous-grid schemes have to use interpolation, which would lead to apparent artificial noises (Aoi and Fujiwara, 1999; Kang and Baag, 2004b). Aoi and Fujiwara (1999) quantitatively evaluate the accuracy of the interpolation in the dis-

Manuscript received by the Editor 1 January 2015; revised manuscript received 27 March 2015; published online 10 June 2015.
[1]Chinese Academy of Sciences, Institute of Geology and Geophysics, Key Laboratory of Earth and Planetary Physics and University of Chinese Academy of Sciences, Beijing, China. E-mail: fannachina@hotmail.com; gaoyingjie@mail.iggcas.ac.cn.
[2]Chinese Academy of Sciences, Institute of Geology and Geophysics, Key Laboratory of Earth and Planetary Physics, Beijing, China. E-mail: zhaolf@mail.iggcas.ac.cn; yaozx@mail.iggcas.ac.cn.

continuous-grid FD method. They conclude that interpolation errors become smaller when the number of grid points per wavelength is larger. For this reason, most discontinuous-grid methods tend to use small grid spacing and those FD schemes with low-order spatial accuracy. Moreover, interpolation errors would be aggravated when wavefield are propagating within the media; therefore, the overall accuracy of the discontinuous-grid FD method would decrease. Some efforts have been made to improve the linear interpolation technique (Wang et al., 2001; Wang and Takenaka, 2001) or to decrease the number of interpolation points using decreasing accurate FD operators toward the border of the fine grid in the transition zones (Kristek et al., 2010). However, neither of these two techniques effectively eliminates the artifacts caused by the interpolation.

In this paper, we present a new discontinuous collocated-grid method for high-order FD modeling. We suggest using a rotated FD operator to avoid using the interpolation. The new scheme retains the accuracy of the continuous-grid scheme and the flexibility and efficiency of the discontinuous-grid scheme. In the "Methodology" section, we describe the methodology of our scheme for the 2D acoustic wave equation. In the "Numerical experiments" section, we demonstrate the accuracy and efficiency of the scheme using a 2D acoustic homogeneous model. The last section of this paper presents our conclusions.

METHODOLOGY

In this section, we illustrate the methodology of the new discontinuous collocated-grid method with the 2D acoustic wave equation, which can be written in the following form:

$$\frac{1}{c^2}\frac{\partial^2 u}{\partial t^2} = \frac{\partial^2 u}{\partial x^2} + \frac{\partial^2 u}{\partial z^2}, \tag{1}$$

where u is the displacement and c is the velocity of the acoustic wave.

As shown in Figure 2, a fine grid is used in the upper region (the area composed of empty squares), whereas a coarse grid is used in the lower region (the area composed of empty circles). The horizontal and vertical spacings are Δx and Δz within the fine-gridded region and $2\Delta x$ and $2\Delta z$ within the coarse-gridded region; i.e., the ratio of the coarse-grid spacing to the fine-grid spacing is 2. Because the horizontal grid spacing is always constant, the second derivatives in the x-direction are approximated using the conventional high-order FD scheme. Difficulties arise in the computation of vertical derivatives, especially near the border between the finely and coarsely gridded regions.

The second derivative in the z-direction on the fine grid is approximated by the conventional high-order FD scheme, which is given by

$$\frac{\partial^2 u}{\partial z^2} \approx \frac{1}{(\Delta z)^2}\sum_{i=1}^{K}\alpha_i[u(x,z+i\Delta z)+u(x,z-i\Delta z) - 2u(x,z)]. \tag{2}$$

The corresponding expression for the coarse grid is

$$\frac{\partial^2 u}{\partial z^2} \approx \frac{1}{(2\Delta z)^2}\sum_{i=1}^{K}\alpha_i[u(x,z+2i\Delta z)+u(x,z-2i\Delta z) - 2u(x,z)], \tag{3}$$

where $2K$ is the order or length of the FD operator, and α_i is the constant coefficient of the conventional FD operator, which can be calculated through the conventional method (Fornberg, 1988) or using the optimization method (Liu and Sen, 2009; Zhang and Yao, 2013a, 2013b).

If the spacings are changed at a depth $z_0 = l\Delta z$ (Figure 2), equation 2 can be used for the FD operator of length $2K$ down to $z = (l-K)\Delta z$ and equation 3 can be used from depth $z = l\Delta z$ downward. At the remaining $(K-1)$ grid points in the transition region (the circumscribed empty squares in Figure 2), the derivative can be approximated as follows (Jastram and Behle, 1992):

$$\begin{aligned}\frac{\partial^2 u}{\partial z^2} \approx{}& \frac{1}{(\Delta z)^2}\sum_{i=1}^{m}\alpha_i^m[u(x,z+i\Delta z) \\ &+ u(x,z-i\Delta z) - 2u(x,z)] \\ &+ \frac{1}{(\Delta z)^2}\sum_{i=m+1}^{K}\alpha_i^m[u(x,z+(m+2(i-m))\Delta z) \\ &+ u(x,z-(m+2(i-m))\Delta z) - 2u(x,z)],\end{aligned} \tag{4}$$

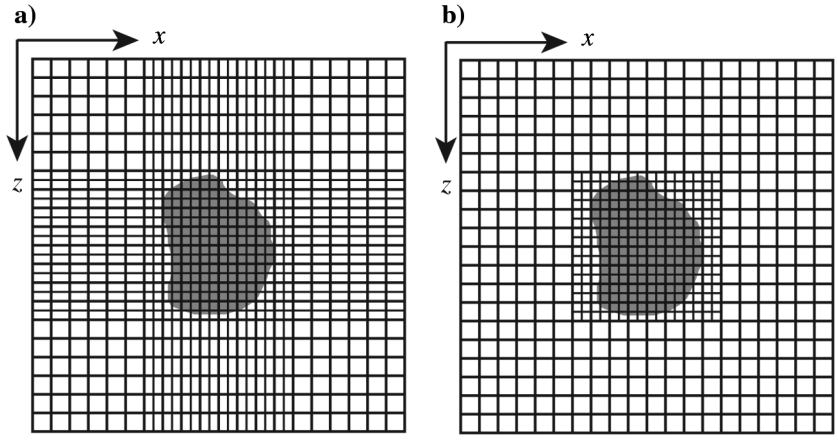

Figure 1. Grid configuration for two types of nonuniform-grid FD modeling methods. The shaded areas represent low-velocity blocks that should be discretized using a fine grid. (a) A continuous-grid scheme requires that the grid points are continuous along both axes throughout the entire region. (b) A discontinuous-grid scheme allows for discontinuous points along grid lines in the transition region but requires interpolation at the positions of the missing points in the coarsely gridded region near the boundary with the finely gridded region.

where m is half of the number of points with small spacing Δz involved in the FD operator and satisfies $m < K$. Figure 2 shows the differencing stencils at selected typical grid point positions in the transition region for the FD operator of length $2K = 6$. The coefficients of the FD operator α_i^m are obtained by solving the following matrix equation (Huang and Dong, 2009):

$$\begin{bmatrix} 1^2 & 2^2 & \cdots & m^2 & (m+N)^2 & \cdots & (m+(i-m)N)^2 & \cdots & (m+(K-m)N)^2 \\ 1^4 & 2^4 & \cdots & m^4 & (m+N)^4 & \cdots & (m+(i-m)N)^4 & \cdots & (m+(K-m)N)^4 \\ \vdots & \vdots & \ddots & \vdots & \vdots & \ddots & \vdots & \ddots & \vdots \\ 1^{2i} & 2^{2i} & \cdots & m^{2i} & (m+N)^{2i} & \cdots & (m+(i-m)N)^{2i} & \cdots & (m+(K-m)N)^{2i} \\ \vdots & \vdots & \ddots & \vdots & \vdots & \ddots & \vdots & \ddots & \vdots \\ 1^{2K} & 2^{2K} & \cdots & m^{2K} & (m+N)^{2K} & \cdots & (m+(i-m)N)^{2K} & \cdots & (m+(K-m)N)^{2K} \end{bmatrix} \begin{bmatrix} \alpha_1^m \\ \alpha_2^m \\ \vdots \\ \alpha_i^m \\ \vdots \\ \alpha_K^m \end{bmatrix} = \begin{bmatrix} 1 \\ 0 \\ \vdots \\ 0 \\ \vdots \\ 0 \end{bmatrix}, \tag{5}$$

where $i = 1,2,3,\cdots,K$ and $N = 2$ is the ratio of the coarse-grid spacing to the fine-grid spacing.

Conventionally, the wavefield of K layers outside the boundary of the fine grid must be interpolated on the coarse grid to calculate the spatial derivatives at discontinuous grid points (e.g., Jastram and Behle, 1992; Zhang et al., 2013). To avoid the artifacts caused by the inaccurate interpolation, we propose a rotated FD operator to avoid interpolation entirely such that high-order spatial accuracy can be retained in the transition region. Similar to the idea of the rotated staggered-grid FD scheme shown in Figure 3, the horizontal and vertical derivatives can be converted into diagonal derivatives (Saenger et al., 2000). The new coordinate system $(\tilde{x},\tilde{z})$ is rotated with respect to the conventional coordinate system (x,z), for which the horizontal and vertical spacings are Δx and Δz, respectively (Figure 3). Thus, we obtain the first and second derivatives:

$$\frac{\partial}{\partial x} = \frac{\Delta r}{2\Delta x}\left(\frac{\partial}{\partial \tilde{x}} - \frac{\partial}{\partial \tilde{z}}\right), \quad \frac{\partial}{\partial z} = \frac{\Delta r}{2\Delta z}\left(\frac{\partial}{\partial \tilde{x}} + \frac{\partial}{\partial \tilde{z}}\right), \tag{6}$$

$$\begin{aligned} \frac{\partial^2}{\partial x^2} &= \frac{\Delta r^2}{4\Delta x^2}\left(\frac{\partial^2}{\partial \tilde{x}^2} + \frac{\partial^2}{\partial \tilde{z}^2} - 2\frac{\partial^2}{\partial \tilde{x}\partial \tilde{z}}\right), \\ \frac{\partial^2}{\partial z^2} &= \frac{\Delta r^2}{4\Delta z^2}\left(\frac{\partial^2}{\partial \tilde{x}^2} + \frac{\partial^2}{\partial \tilde{z}^2} + 2\frac{\partial^2}{\partial \tilde{x}\partial \tilde{z}}\right), \end{aligned} \tag{7}$$

where $\Delta r = \sqrt{(\Delta x)^2 + (\Delta z)^2}$.

As is usually the case, $\Delta x = \Delta z$; thus, for the 2D acoustic wave equation, we obtain

$$\frac{\partial^2 u}{\partial x^2} + \frac{\partial^2 u}{\partial z^2} = \frac{\partial^2 u}{\partial \tilde{x}^2} + \frac{\partial^2 u}{\partial \tilde{z}^2}. \tag{8}$$

The second derivatives in the new coordinate system $(\tilde{x},\tilde{z})$ are approximated using the following high-order FD scheme:

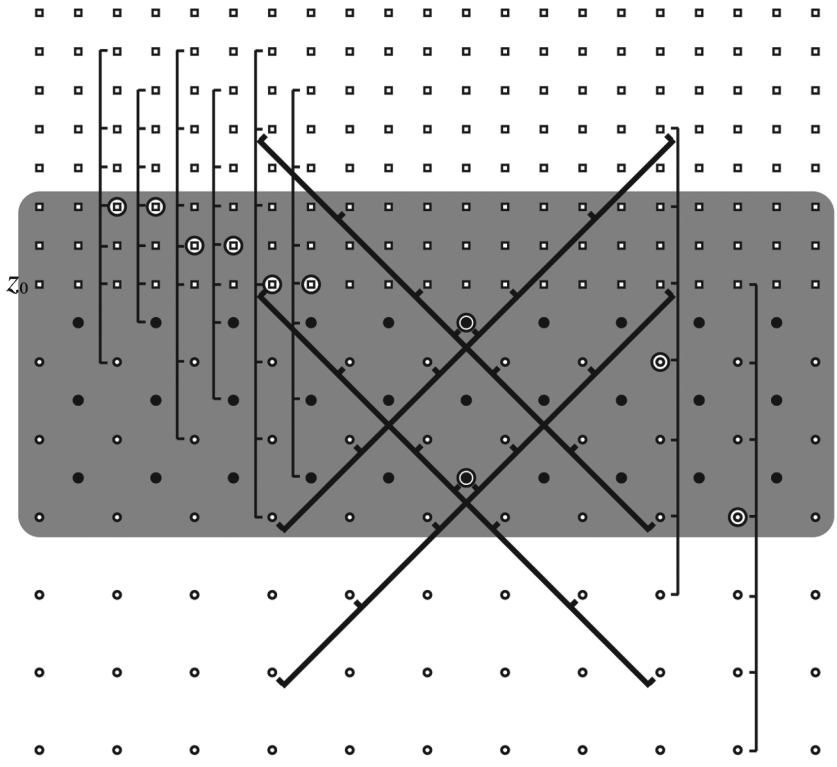

Figure 2. Grid configuration for the proposed scheme of refining the wavefield on a rotated coordinate system. A fine grid (empty squares) is used in the upper region, and a coarse grid (empty circles) is used in the lower region. The horizontal and vertical spacings are Δx and Δz within the finely gridded region and $2\Delta x$ and $2\Delta z$ within the coarsely gridded region. The shaded area represents the transition zone, in which the fine and coarse grids meet with a spatial accuracy of $2K = 6$. Differencing stencils of the vertical derivatives for several typical points (circumscribed empty squares and circumscribed solid circles) in the transition zone are shown. At the missing grid points (solid circles), we use the rotated FD operator to calculate the horizontal and vertical derivatives.

$$\frac{\partial^2 u}{\partial \tilde{x}^2} \approx \frac{1}{(\Delta r)^2}\alpha_i^1[u(x+i\Delta x, z+i\Delta z) + u(x-i\Delta x, z-i\Delta z) - 2u(x,z)] + \frac{1}{(\Delta r)^2}\sum_{i=2}^{K}\alpha_i^1[u(x+(2i-1)\Delta x, z+(2i-1)\Delta z) + u(x-(2i-1)\Delta x, z-(2i-1)\Delta z) - 2u(x,z)], \quad (9)$$

$$\frac{\partial^2 u}{\partial \tilde{z}^2} \approx \frac{1}{(\Delta r)^2}\alpha_i^1[u(x+i\Delta x, z-i\Delta z) + u(x-i\Delta x, z+i\Delta z) - 2u(x,z)] + \frac{1}{(\Delta r)^2}\sum_{i=2}^{K}\alpha_i^1[u(x+(2i-1)\Delta x, z-(2i-1)\Delta z) + u(x-(2i-1)\Delta x, z+(2i-1)\Delta z) - 2u(x,z)], \quad (10)$$

in which the constant coefficients α_i^1 are the solutions to equation 5 for $m = 1$. The spatial accuracy is still $2K$. Therefore, the vertical and horizontal derivatives at all of the missing points (solid circles in Figure 2) can be obtained using the rotated FD operator described in equations 9 and 10. In summary, we can obtain the spatial derivatives at all points in the transition region with $2K$-order spatial accuracy.

The temporal derivatives in equation 1 are obtained using the second-order conventional FD operator:

$$\frac{\partial^2 u}{\partial t^2} \approx \frac{1}{(\Delta t)^2}[(t+\Delta t) + u(t-\Delta t) - 2u(t)]. \quad (11)$$

We have illustrated the methodology of discontinuous collocated-grid FD modeling for a spacing ratio $N = 2$, but we find that this method does not extend to $N = 3$. However, the scheme for $N = 2$ can be repeated n times to achieve $N = 2^n$. The methodology for $N = 2^n$ is illustrated in Figure 4. Note that beneath every boundary between grids with different spacings, a buffer zone must exist. For example, when transitioning from a spacing of $2^i\Delta x$ to $2^{i+1}\Delta x$, a buffer layer of minimal size $(2K-1)2^{i+1}\Delta x$ must exist in the coarser grid. Figure 4 shows the setup for a spacing change from Δx to $8\Delta x$ with a spatial accuracy of $2K = 6$.

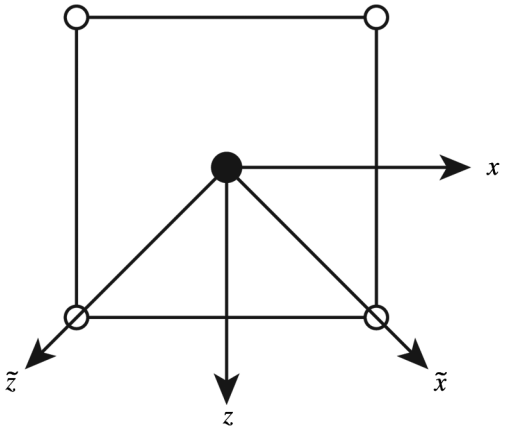

Figure 3. The rotated coordinates used in our scheme. The conventional 2D Cartesian coordinate system (x, z) is rotated to a new coordinate system $(\tilde{x}, \tilde{z})$ with horizontal and vertical spacings of Δx and Δz, respectively.

Nonreflecting boundaries are needed in realistic simulations. Here, we apply the perfectly matched layer (PML) as the absorbing boundary. The PML equations for the 2D acoustic wave equation are written as follows (Liu et al., 2012):

$$\left(\frac{\partial}{\partial t} + d(x)\right)^2 u_1 = c^2\left(\frac{\partial^2 u}{\partial x^2} + P_1\right),$$
$$\left(\frac{\partial}{\partial t} + d(z)\right)^2 u_2 = c^2\left(\frac{\partial^2 u}{\partial z^2} + P_2\right),$$
$$\left(\frac{\partial}{\partial t} + d(x)\right) P_1 = -d'(x)\frac{\partial u}{\partial x},$$
$$\left(\frac{\partial}{\partial t} + d(z)\right) P_2 = -d'(z)\frac{\partial u}{\partial z}, \quad (12)$$

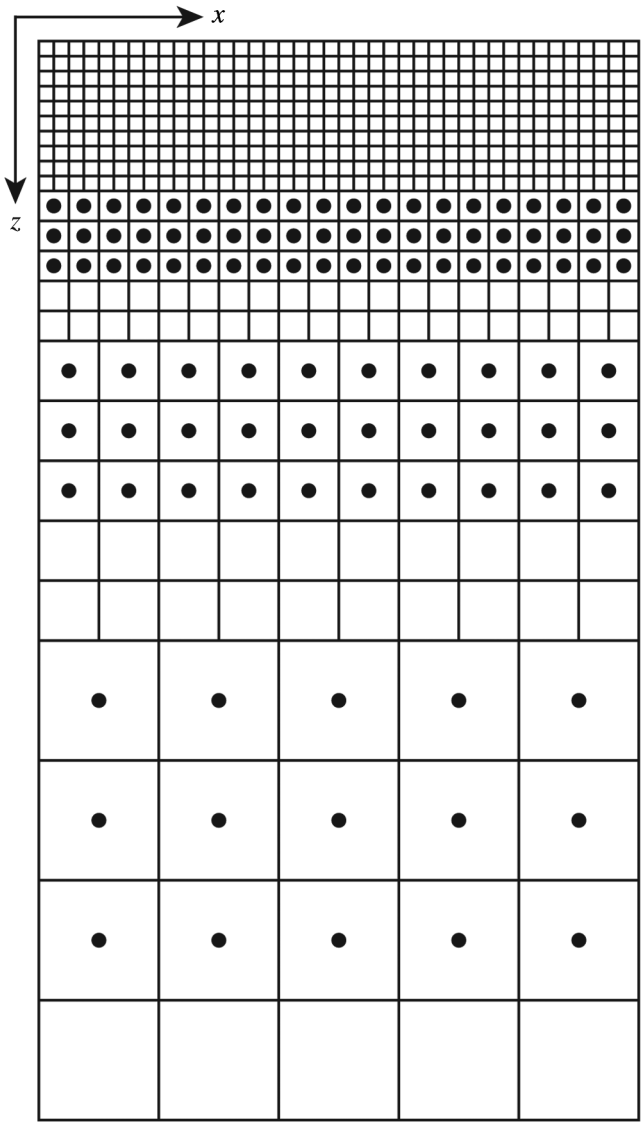

Figure 4. Grid configuration in the case of grid spacing changing from Δx to $8\Delta x$. The spatial accuracy of the FD operator is of $2K = 6$. The solid circles denote the positions of points at which rotated FD operators are used to calculate the horizontal and vertical derivatives.

where u_1 and u_2 are the splitting wavefields, $u = u_1 + u_2$, P_1 and P_2 are the auxiliary variables, $d(x)$ and $d(z)$ are the damping functions (Collino and Tsogka 2001), and $d'(x)$ and $d'(z)$ are the spatial first derivatives of $d(x)$ and $d(z)$, respectively. We use a damping function

$$d(x) = \frac{3c}{2\delta}\log\left(\frac{1}{R}\right)\left(\frac{x}{\delta}\right)^2, \tag{13}$$

where $R = 0.001$, x is the distance from the point of interest to the PML interface with the interior region, and δ is the thickness of the PML layers.

The spatial first derivative in equation 12 in the transition zone of the PML layers can be approximated by

$$\begin{aligned}\frac{\partial u}{\partial z} \approx & \frac{1}{\Delta z}\sum_{i=1}^{m}\beta_i^m[u(x,z+i\Delta z) - u(x,z-i\Delta z)] \\ & + \frac{1}{\Delta z}\sum_{i=m+1}^{K}\beta_i^m[u(x,z+(m+2(i-m))\Delta z) \\ & - u(x,z-(m+2(i-m))\Delta z)],\end{aligned} \tag{14}$$

where the coefficients β_i^m are calculated using the following equation:

$$\begin{bmatrix} 1 & 2 & \cdots & m & (m+N) & \cdots & (m+(i-m)N) & \cdots & (m+(K-m)N) \\ 1^3 & 2^3 & \cdots & m^3 & (m+N)^3 & \cdots & (m+(i-m)N)^3 & \cdots & (m+(K-m)N)^3 \\ \vdots & \vdots & \ddots & \vdots & \vdots & \ddots & \vdots & \ddots & \vdots \\ 1^{2i-1} & 2^{2i-1} & \cdots & m^{2i-1} & (m+N)^{2i-1} & \cdots & (m+(i-m)N)^{2i-1} & \cdots & (m+(K-m)N)^{2i-1} \\ \vdots & \vdots & \ddots & \vdots & \vdots & \ddots & \vdots & \ddots & \vdots \\ 1^{2K-1} & 2^{2K-1} & \cdots & m^{2K-1} & (m+N)^{2K-1} & \cdots & (m+(i-m)N)^{2K-1} & \cdots & (m+(K-m)N)^{2K-1} \end{bmatrix} \times \begin{bmatrix} \beta_1^m \\ \beta_2^m \\ \vdots \\ \beta_i^m \\ \vdots \\ \beta_K^m \end{bmatrix} = \begin{bmatrix} \frac{1}{2} \\ 0 \\ \vdots \\ 0 \\ \vdots \\ 0 \end{bmatrix}. \tag{15}$$

As in the calculation of the spatial second derivatives using the rotated FD operator, we use equations 6 and 14 to obtain the first derivatives in the PML layers.

The total thickness of the PML layers is the same within both the fine and coarse grids. For example, for a grid spacing ratio of $N = 2$, if the number of PML layers in the coarse grid is 20, then the number in the fine grid is 40. The first layer of the PML should be aligned within the fine and coarse grids. Thus, the damping functions $d(x)$ on each PML layers are the same, which guarantees similar absorbing effects on the discontinuous grid.

Because we merely replace the interpolation operator with the rotated FD operator at the missing points, the computational costs

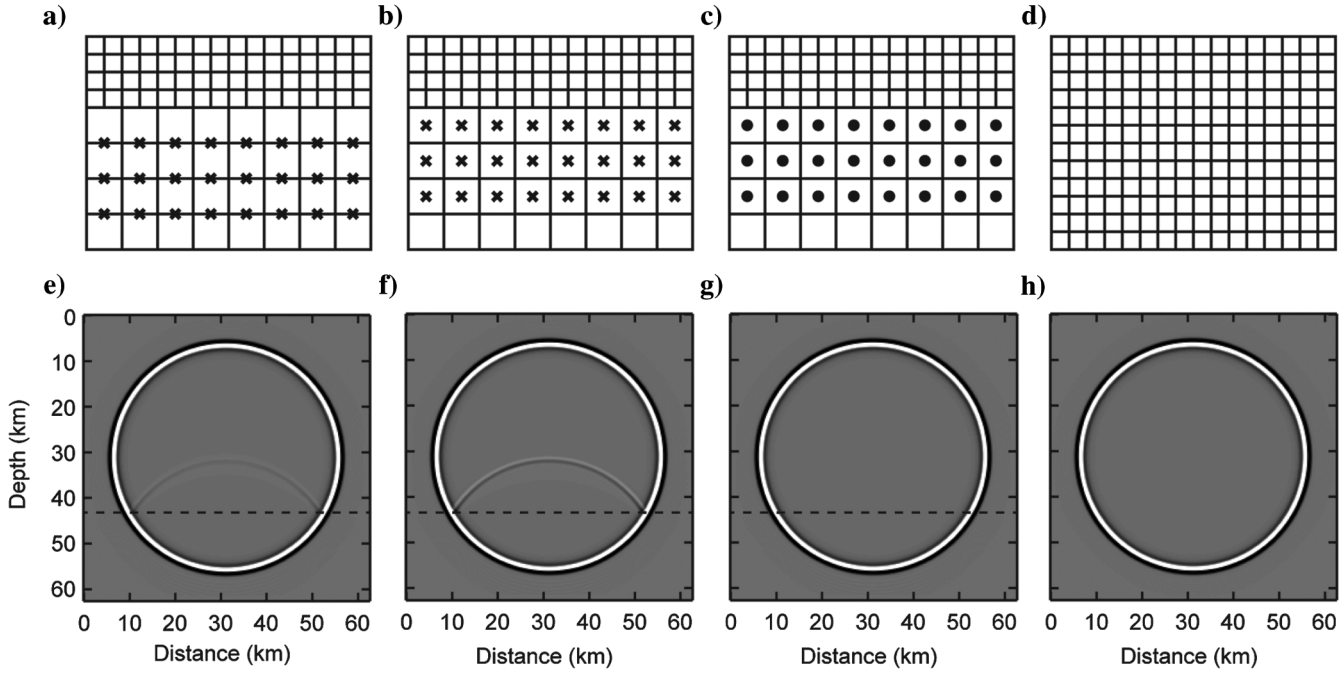

Figure 5. Snapshots of the wavefield (e-h) at a traveltime of 13.6 s. These wavefields are calculated by interpolation scheme 1 (a), interpolation scheme 2 (b), our rotated FD scheme (c) and the uniform-grid scheme (d), respectively. The black crosses in (a and b) denote the grid points at which the wavefield values are interpolated, and the solid circles in (c) denote the grid points at which the wavefield values are calculated using the rotated FD operator. Fine and coarse grids are used in the upper and lower regions, respectively, and the boundary of the two subregions is located at a depth of $z = 43.75$ km (indicated by the dashed lines in [e-g]).

of the two methods are almost the same for $N = 2$. For $N > 2$, some buffer layers exist. However, in practice, values of $N = 2$ or 4 are most commonly used. Consequently, the buffer layers are relatively small compared with the entire model domain, and thus the added computational expense is negligible.

NUMERICAL EXPERIMENTS

To demonstrate the accuracy of our discontinuous-grid method, we compare our scheme with the interpolation scheme and the uniform-grid FD scheme by performing numerical tests with a 2D homogeneous acoustic model. The size of the model is 62.5×62.5 km^2, and the wave velocity is $c = 2000$ m/s. The upper region uses a small grid spacing of $\Delta x = \Delta z = 125$ m, and the lower region uses a large grid spacing of $2\Delta x$. The boundary of the two subregions is located at a depth of $z = 43.75$ km (which is indicated by the dashed lines in Figure 5e–5g). The source is located at the center of the model domain (31.25 km, 31.25 km). The source time function is a Ricker wavelet with a center frequency of 1.0 Hz and a time shift of 1.2 s.

We compare the simulation snapshots using four different FD schemes: interpolation scheme 1 (Figure 5a) (Jastram and Behle, 1992), interpolation scheme 2 (Figure 5b), the rotated FD scheme (Figure 5c), and the uniform-grid scheme (Figure 5d). The crosses in Figure 5a and 5b denote missing grid points at which interpolation is performed. The interpolation technique used in our study is linear interpolation. The solid circles in Figure 5c denote the missing grid points at which a rotated FD operator is used. All the different FD schemes in Figure 5a–5d are with a tenth-order spatial accuracy and second-order temporal accuracy for solving the 2D acoustic wave equation. Figure 5e–5h shows snapshots of the wavefield at a time of 13.6 s calculated by the different FD schemes shown in Figure 5a–5d. The interpolation scheme introduces obvious artificial noises (Figure 5e and 5f) that are reflected off of the interface of the spacing change (the dashed lines in Figure 5e and 5f); these reflections do not appear in the rotated FD scheme (Figure 5g), and the uniform-grid FD scheme (Figure 5h). Figure 5g suggests that our scheme effectively reduces the artificial reflections. Figure 6a compares four seismograms at the same location (31.25 km, 25 km) using interpolation scheme 1 (black dashed line), interpolation scheme 2 (gray dotted line), the rotated FD scheme (gray solid line), and the uniform-grid scheme (black solid line). Artificial reflections emerge at approximately 17 s and have amplitudes that are much less than that of the direct wave. However, if one or more velocity-change interfaces exist in the model, these artificial reflections are significant compared with the real reflections and thus cannot be ignored in practical applications. Figure 6b shows a magnified view of the region in which the artificial reflections occur (dashed box in Figure 6a). The maximum amplitudes of the seismograms between 16 and 18.5 s are 0.025390 (interpolation scheme 1), 0.085223 (interpolation scheme 2), 2.7769×10^{-04} (rotated FD scheme), 2.0304×10^{-04}(uniform-grid scheme) respectively. It is obvious that the two interpolation schemes both produce artificial reflections and the reflection of scheme 2 is larger than that of scheme 1. Our scheme produces no artificial reflection and yields a wavefield that is almost identical to that of the uniform-grid simulation.

Similar to the results of the stability tests of the discontinuous grid in the collocated-grid FD method that uses the dispersion relation preserving/optimization (DRP/opt) MacCormack scheme described in Zhang et al. (2013), we find that our scheme remains

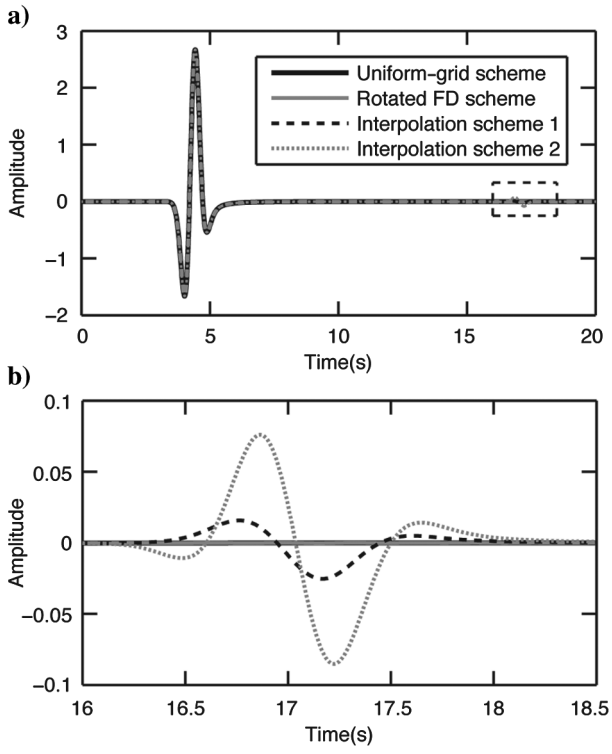

Figure 6. (a) Seismograms measured by a receiver using different methods. The results are obtained from interpolation scheme 1 (black dashed line), interpolation scheme 2 (gray dotted line), our rotated FD scheme (gray solid line), and the uniform-grid scheme (black solid line). The direct waves arrive at approximately 4 s, and artificial reflections emerge at approximately 17 s. The amplitudes of the artificial reflections are much less than that of the direct wave. (b) A magnified view of the amplified artificial reflections in the dashed box of (a).

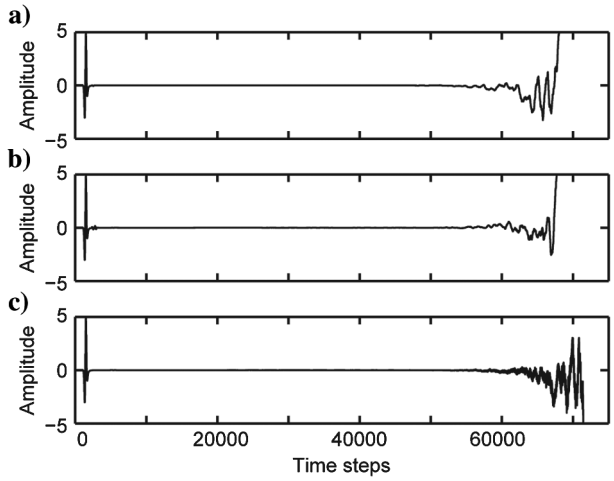

Figure 7. Numerical stability tests for a grid spacing ratio of$N = 4$. (a-c) Seventy-five thousand time steps using interpolation schemes 1 and 2 and the rotated FD scheme, respectively. The seismograms are truncated when the amplitudes of the instability reach the maximum amplitude of the direct wave.

stable over long time periods for a grid-spacing ratio $N = 2$ in a homogeneous medium. Instability problems occur only with large grid-spacing ratios ($N > 2$). We implement another numerical test for a grid-spacing ratio of $N = 4$; in this case, the grid spacing must change twice within our scheme. Figure 7 shows the results of 75,000 time steps using interpolation schemes 1 (Figure 7a) and 2 (Figure 7b) and our rotated FD scheme (Figure 7c). It is obvious that our scheme suffers from an instability problem like the other method, although it is not that serious. Kristek et al. (2010) note that such instabilities primarily result from small-wavelength signal components in the fine grid that cannot propagate into the coarse grid. To solve the instability problem, Kristek et al. (2010) introduce a Lanczos filter for a 3D staggered-grid FD scheme. However, Zhang et al. (2013) find that the Lanczos filter is not compatible with the collocated-grid DRP/opt MacCormack scheme and introduce a Gaussian filter instead. It seems that a general downsampling filter that can work with different FD schemes does not exist. We tested these two downsampling filters and found that neither works with our scheme. Thus, in future work, a proper downsampling filter should be determined to solve the instability problem.

CONCLUSIONS

Conventional discontinuous-grid FD modeling uses the interpolation to obtain the wavefield at missing grid points in the transition region; however, the interpolation greatly decreases the computational accuracy due to apparent artificial reflections from the boundary of the two grid systems. We present a new discontinuous collocated-grid scheme for high-order FD modeling that uses a rotated FD operator at the missing grid points. We illustrate the scheme by solving the 2D acoustic wave equation. The ratio of the coarse-grid spacing to fine-grid spacing is restricted to 2^n, where n is a positive integer. By comparing our results with those of interpolation schemes in a 2D homogeneous acoustic medium, we find that our scheme effectively reduces artificial reflections with minimal extra computational costs. However, our scheme exhibits instability problems like traditional methods. Extension of the 2D acoustic implementation of our scheme to 2D and 3D elastic modeling is straightforward and exhibits no additional technical problems.

ACKNOWLEDGMENTS

The authors thank the two anonymous reviewers for their insightful comments and suggestions, which greatly improved the manuscript. Fruitful discussions with Y.-S. Liu are also gratefully appreciated. The work is supported by the National Natural Science Foundation of China (grant nos. 41374065 and 41174048).

REFERENCES

Aoi, S., and H. Fujiwara, 1999, 3D finite-difference method using discontinuous grids: Bulletin of the Seismological Society of America, **89**, 918–930.

Collino, F., and C. Tsogka, 2001, Application of the perfectly matched absorbing layer model to the linear elastodynamic problem in anisotropic heterogeneous media: Geophysics, **66**, 294–307, doi: 10.1190/1.1444908.

Falk, J., E. Tessmer, and D. Gajewski, 1996, Tube wave modeling by the finite-difference method with varying grid spacing: Pure and Applied Geophysics, **148**, 77–93, doi: 10.1007/BF00882055.

Fornberg, B., 1988, Generation of finite difference formulas on arbitrarily spaced grids: Mathematics of Computation, **51**, 699–706, doi: 10.1090/S0025-5718-1988-0935077-0.

Hayashi, K., D. R. Burns, and M. N. Toksöz, 2001, Discontinuous-grid finite-difference seismic modeling including surface topography: Bulletin of the Seismological Society of America, **91**, 1750–1764, doi: 10.1785/0120000024.

Huang, C., and L. G. Dong, 2009, High-order finite-difference method in seismic wave simulation with variable grids and local time-steps: (in Chinese) Chinese Journal of Geophysics, **52**, 176–187, doi: 10.1002/cjg2.1338.

Jastram, C., and A. Behle, 1992, Acoustic modelling on a grid of vertically varying spacing: Geophysical Prospecting, **40**, 157–169, doi: 10.1111/j.1365-2478.1992.tb00369.x.

Jastram, C., and E. Tessmer, 1994, Elastic modelling on a grid with vertically varying spacing: Geophysical Prospecting, **42**, 357–370, doi: 10.1111/j.1365-2478.1994.tb00215.x.

Kang, T. S., and C. E. Baag, 2004a, An efficient finite-difference method for simulating 3D seismic response of localized basin structures: Bulletin of the Seismological Society of America, **94**, 1690–1705, doi: 10.1785/012004016.

Kang, T. S., and C. E. Baag, 2004b, Finite-difference seismic simulation combining discontinuous grids with locally variable timesteps: Bulletin of the Seismological Society of America, **94**, 207–219, doi: 10.1785/0120030080.

Kristek, J., P. Moczo, and M. Galis, 2010, Stable discontinuous staggered grid in the finite-difference modelling of seismic motion: Geophysical Journal International, **183**, 1401–1407, doi: 10.1111/j.1365-246X.2010.04775.x.

Liu, X., X. Yin, and G. Wu, 2014, Finite-difference modeling with variable grid-size and adaptive time-step in porous media: Earthquake Science, **27**, 169–178, doi: 10.1007/s11589-013-0055-7.

Liu, Y., and M. K. Sen, 2009, A new time–space domain high-order finite-difference method for the acoustic wave equation: Journal of Computational Physics, **228**, 8779–8806, doi: 10.1016/j.jcp.2009.08.027.

Liu, Y. S., S. L. Liu, M. G. Zhang, and D. T. Ma, 2012, An improved perfectly matched layer absorbing boundary condition for second order elastic wave equation: (in Chinese) Progress in Geophysics, **27**, 2113–2122.

Moczo, P., P. Labák, J. Kristek, and F. Hron, 1996, Amplification and differential motion due to an antiplane 2D resonance in the sediment valleys embedded in a layer over the half-space: Bulletin of the Seismological Society of America, **86**, 1434–1446.

Opršal, I., and J. Zahradnik, 1999, Elastic finite-difference method for irregular grids: Geophysics, **64**, 240–250, doi: 10.1190/1.1444520.

Pitarka, A., 1999, 3D elastic finite-difference modeling of seismic motion using staggered grids with nonuniform spacing: Bulletin of the Seismological Society of America, **89**, 54–68.

Saenger, E. H., N. Gold, and S. A. Shapiro, 2000, Modeling the propagation of elastic waves using a modified finite-difference grid: Wave Motion, **31**, 77–92, doi: 10.1016/S0165-2125(99)00023-2.

Wang, Y., and G. T. Schuster, 1996, Finite-difference variable grid scheme for acoustic and elastic wave equation modeling: 66th Annual International Meeting, SEG, Expanded Abstracts, 674–677.

Wang, Y., J. Xu, and G. T. Schuster, 2001, Viscoelastic wave simulation in basins by a variable-grid finite-difference method: Bulletin of the Seismological Society of America, **91**, 1741–1749, doi: 10.1785/0120000236.

Wang, Y. B., and H. Takenaka, 2001, A multidomain approach of the Fourier pseudospectral method using discontinuous grid for elastic wave modeling: Earth, Planets and Space, **53**, 149–158, doi: 10.1186/BF03352372.

Wu, C., J. M. Harris, K. T. Nihei, and S. Nakagawa, 2005, Two-dimensional finite-difference seismic modeling of an open fluid-filled fracture: Comparison of thin-layer and linear-slip models: Geophysics, **70**, no. 4, T57–T62, doi: 10.1190/1.1988187.

Zhang, J. H., and Z. X. Yao, 2013a, Optimized explicit finite-difference schemes for spatial derivatives using maximum norm: Journal of Computational Physics, **250**, 511–526, doi: 10.1016/j.jcp.2013.04.029.

Zhang, J. H., and Z. X. Yao, 2013b, Optimized finite-difference operator for broadband seismic wave modeling: Geophysics, **78**, no. 1, A13–A18, doi: 10.1190/geo2012-0277.1, doi: 10.1190/geo2012-0277.1.

Zhang, W., Y. Shen, and X. F. Chen, 2008, Numerical simulation of strong ground motion for the M s8. 0 Wenchuan earthquake of 12 May 2008: Science in China, Series D: Earth Sciences, **51**, 1673–1682, doi: 10.1007/s11430-008-0130-4.

Zhang, Z. G., W. Zhang, H. Li, and X. F. Chen, 2013, Stable discontinuous grid implementation for collocated-grid finite-difference seismic wave modelling: Geophysical Journal International, **192**, 1179–1188, doi: 10.1093/gji/ggs069.